Laminar Flow in Isosceles Triangular Ducts

E. M. SPARROW

University of Minnesota, Minneapolis, Minnesota

The fluid flow characteristics of noncircular ducts have become a subject of considerable practical interest in recent years, especially in connection with compact heat exchange equipment. The noncircular configuration of particular interest here is the duct of triangular cross section. For laminar flow conditions analysis has been able to provide exact solutions for the fully developed velocity distribution and friction factor only for the right-isosceles* and for the equilateral triangle (*1, 2*). For isosceles ducts of other opening angles approximate friction factors of uncertain accuracy have been derived utilizing the Raleigh-Ritz variational method (*3*). Detailed aspects of the flow (such as the velocity profile and the distribution of local wall shear stress) could not be obtained with the approximate solution method. The need for such detailed velocity information as input to a heat transfer analysis motivated the consideration of a circular sector duct as a substitute for the triangular cross section (*4*). The velocity solution for this circular sector is in the form of an infinite series.

The present investigation aims to obtain highly accurate laminar velocity solutions for isosceles ducts which will provide both detailed (velocity profiles, wall shear distributions) and overall (friction factor) information. This will be accomplished by applying a new solution method (*5*). The velocity profiles are in the form of finite series and are thus convenient for later application to heat transfer studies.

Experiments on the fluid flow characteristics of triangular ducts are reported in references *6* to *11*, and pertinent data from these references will be compared with the present analytical results. An analysis of turbulent flow in triangular ducts has been carried out in reference *12*.

A cross-sectional view of an isosceles triangular duct is shown in Figure 1 along with dimensional nomenclature. The coordinates r and θ are standard polar coordinates. The opening angle of the duct is 2α, while s represents the height measured from the apex.

ANALYSIS

The Governing Equation and Its Solution

The starting point of the analysis is the conservation of momentum principle. For fully developed isothermal flow there is no change of momentum as the fluid flows through the duct. Therefore the conservation law reduces to a balance between pressure forces and viscous forces. It is convenient for later analysis to write the force balance in cylindrical coordinates (for example reference *1*, Equations 4-33)

$$\frac{dp}{dx} = \mu\left(\frac{\partial^2 u}{\partial r^2} + \frac{1}{r}\frac{\partial u}{\partial r} + \frac{1}{r^2}\frac{\partial^2 u}{\partial \theta^2}\right) \tag{1}$$

where dp/dx, the axial pressure drop, is constant and negative for fully developed flow conditions. If Equation (1) can be solved subject to the no-slip condition that u is zero on all duct boundaries, then all flow quantities of interest can be determined. The interesting and challenging aspect of the problem is that the triangular cross section does not lend itself naturally to analysis either in rectangular or in cylindical coordinates.

In approaching the task of solving Equation (1) perhaps the most reasonable beginning is to reduce it to Laplace's equation, which is the most familiar and perhaps best understood of any partial differential equation. Thus there is introduced a reduced velocity u^*:

$$u = u^* + \frac{r^2}{4}\left(\frac{1}{\mu}\frac{dp}{dx}\right) \tag{2}$$

After substituting in Equation (1) one finds that u^* must satisfy Laplace's equation:

$$\frac{\partial^2 u^*}{\partial r^2} + \frac{1}{r}\frac{\partial u^*}{\partial r} + \frac{1}{r^2}\frac{\partial^2 u^*}{\partial \theta^2} = 0 \tag{3}$$

There are of course a great many well-known solutions of Laplace's equation, any number of which may be added together to satisfy the boundary condition $u = 0$. One group of solutions is usually found by the separation of variables method, whereby u^* is taken in the form of a product $u^* = R(r)\cdot\Theta(\theta)$, where R is a function of r alone and Θ is a function of θ alone. The separation of variables method is described in standard books on advanced calculus and leads to the solution (*13*, p. 424):

$$u^* = (A_o + B_o \ln r)(C_o + D_o\theta) + \sum_k (A_k r^k + B_k r^{-k}) \cdot (E_k \cos k\theta + D_k \sin k\theta) \tag{4}$$

In the present application, where it is required that the velocity is finite everywhere and in particlular at $r = 0$, it follows that

$$B_o = 0, \qquad B_k = 0 \tag{4a}$$

Additionally since there is symmetry about the line $\theta = 0$

$$D_o = 0, \qquad D_k = 0 \tag{4b}$$

If one utilizes these facts to simplify Equation (4) and then substitutes the resulting expression for u^* into Equation (2), there is obtained ($E_k = 1$ without loss of generality)

$$u = A_oC_o + \frac{r^2}{4}\left(\frac{1}{\mu}\frac{dp}{dx}\right) + \sum_k A_k r^k \cos k\theta \tag{5}$$

The remaining constants are determined by imposing the condition that $u = 0$ on all boundaries. To satisfy this requirement at $r = 0$ it is necessary that $A_oC_o = 0$. Next, when one applies Equation (5) on the oblique sides $\theta = \pm\alpha$ (see Figure 1)

$$0 = \frac{r^2}{4}\left(\frac{1}{\mu}\frac{dp}{dx}\right) + \sum_k A_k r^k \cos k\alpha \tag{6a}$$

This may be satisfied by taking $\cos k\alpha = 0$, from which it follows that $k\alpha = \pi/2, 3\pi/2, \ldots$, or

$$k = \frac{(2n-1)\pi}{2\alpha}, \quad n = 1, 2, 3, \ldots \tag{6b}$$

and also, to cancel the term

$$(r^2/4)\left(\frac{1}{\mu}\frac{dp}{dx}\right)$$

it is necessary to take $k = 2$ and

$$A_{k=2} = \frac{1}{4\cos 2\alpha}\left(\frac{1}{\mu}\frac{dp}{dx}\right) \tag{6c}$$

With these the velocity solution (5) becomes

$$u \Big/ \left(-\frac{1}{4\mu}\frac{dp}{dx}\right) = r^2\left(\frac{\cos 2\theta}{\cos 2\alpha} - 1\right) + \sum_{n=1}^{\frac{(2n-1)\pi}{2\alpha}} A_n r^{\frac{(2n-1)\pi}{2\alpha}} \cos\left[\frac{(2n-1)\pi\theta}{2\alpha}\right] \tag{7}$$

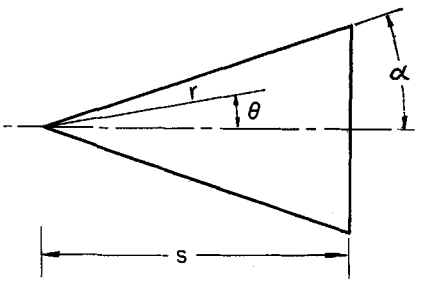

Fig. 1. Cross section of isosceles triangular duct.

* In this case the velocity solution is an infinite series.

TABLE 1. LISTING OF C_n VALUES

α	C_1	C_2	C_3	C_4	C_5	C_6	C_7	C_8	C_9	C_{10}
5°	−0.01577	$0.4027\cdot10^{-3}$	$-0.6979\cdot10^{-4}$	$0.2108\cdot10^{-4}$	$-0.834\cdot10^{-5}$	$0.386\cdot10^{-5}$	$-0.199\cdot10^{-5}$	$0.109\cdot10^{-5}$	$-0.63\cdot10^{-6}$	$0.38\cdot10^{-6}$
10°	−0.06514	$0.1086\cdot10^{-2}$	$-0.1486\cdot10^{-3}$	$0.3692\cdot10^{-4}$	$-0.122\cdot10^{-4}$	$0.478\cdot10^{-5}$	$-0.209\cdot10^{-5}$	$0.99\cdot10^{-6}$	$-0.49\cdot10^{-6}$	$0.25\cdot10^{-6}$
15°	−0.1561	$0.1563\cdot10^{-2}$	$-0.1650\cdot10^{-3}$	$0.3331\cdot10^{-4}$	$-0.913\cdot10^{-5}$	$0.300\cdot10^{-5}$	$-0.111\cdot10^{-5}$	$0.44\cdot10^{-6}$	$-0.19\cdot10^{-6}$	$0.75\cdot10^{-7}$
20°	−0.3069	$0.1596\cdot10^{-2}$	$-0.1257\cdot10^{-3}$	$0.2025\cdot10^{-4}$	$-0.4554\cdot10^{-5}$	$0.124\cdot10^{-5}$	$-0.39\cdot10^{-6}$	$0.12\cdot10^{-6}$	$-0.5\cdot10^{-7}$	$0.1\cdot10^{-7}$
22.5°	−0.4155	$0.1411\cdot10^{-2}$	$-0.9415\cdot10^{-4}$	$0.1347\cdot10^{-4}$	$-0.272\cdot10^{-5}$	$0.67\cdot10^{-6}$	$-0.19\cdot10^{-6}$	$0.5\cdot10^{-7}$	$-0.3\cdot10^{-7}$	
25°	−0.5568	$0.1083\cdot10^{-2}$	$-0.6024\cdot10^{-4}$	$0.759\cdot10^{-5}$	$-0.14\cdot10^{-5}$	$0.3\cdot10^{-6}$	$-0.9\cdot10^{-7}$	$0.2\cdot10^{-7}$	$-0.2\cdot10^{-7}$	
30°	−1	0	0	0	0	0	0	0	0	
35°	−1.922	$-0.1630\cdot10^{-2}$	$0.306\cdot10^{-4}$	$-0.234\cdot10^{-5}$	$0.3\cdot10^{-6}$	$-0.6\cdot10^{-7}$				
40°	−4.755	$-0.3748\cdot10^{-2}$	$0.157\cdot10^{-4}$	$-0.17\cdot10^{-5}$	$0.1\cdot10^{-6}$	$-0.6\cdot10^{-7}$				

The set of constants A_n still remains to be found, and for this there is available the condition that $u = 0$ on the right-hand boundary (Figure 1) of the duct. Now, on this boundary, r and θ are related by

$$r = s/\cos\theta \tag{8}$$

The introduction of this into Equation (7) and the setting of $u = 0$ leads to

$$\frac{1}{(\cos\theta)^2}\left(1-\frac{\cos 2\theta}{\cos 2\alpha}\right) = \sum_{n=1} C_n \frac{\cos[(2n-1)\pi\theta/2\alpha]}{[\cos\theta]^{(2n-1)\pi/2\alpha}} \tag{9}$$

where the C_n are the dimensionless counterparts of the constants A_n, that is

$$C_n = A_n s^{\frac{(2n-1)\pi}{2\alpha}-2} \tag{10}$$

The pivotal point in the analysis is the determination of the C_n. As a first approach it is natural to consider the methods of Fourier series. But this procedure will not apply in the present problem for the mathematical reason that the functions $\cos[(2n-1)\pi\theta/2\alpha]\cdot[\cos\theta]^{-\frac{(2n-1)\pi}{2\alpha}}$ do not form a complete orthogonal set. This inapplicability of the Fourier methods is also physically plausible since the boundaries of the triangular duct do not fully fit into either a rectangular or a cylindrical coordinate system.*

The method used for finding the C_n is based on the application of Equation (9) at a finite number of points along the boundary (5). Suppose for example that one decides to satisfy Equation (9) at M locations. Then M values of θ in the range $0 \leq \theta < \alpha$ are selected, and Equation (9) is evaluated at each one of these θ values, thus providing M equations. Additionally if the series appearing in Equation (9) is truncated after M terms, there are M unkonwn coefficients C_n. The set of M linear inhomogeneous algebraic equations can be solved to yield the M unknown C_n. To check the accuracy of the coefficients thus obtained the entire procedure may be repeated by satisfying the condition (9) at $(M+1)$ locations on the boundary and truncating after $(M+1)$ terms. Further information may be obtained by utilizing $(M+2)$ boundary points, $(M+3)$ boundary points, and so forth. Then by comparing the sets of coefficients from these various calculations one sees certain important characteristics.

It is found that if sufficient boundary points are used, the first several C_n are independent of both the number of boundary points and their location. In other words if Equation (9) were to be satisfied at additional boundary points, the first several C_n would not be altered. Thus the first several C_n obtained in this way may be regarded as truly characteristic of the solution. In principle it is possible to arrive at as large a group of these invariant C_n as are desired by satisfying Equation (9) at a sufficiently large number of points. However in practice there is a limitation imposed by the loss of significant figures which results when large numbers of linear algebraic equations are solved numerically.

Another important characteristic of the C_n is that they decrease rapidly with increasing n. This is of great practical consequence, because only the first several C_n are needed in order to compute velocity profiles, wall shear stress distributions, and the friction factor-Reynolds number relationship. It thus follows that an accurate knowledge of the first several C_n is essentially equivalent to a solution of the velocity problem.

Inspection of Equation (9) reveals that the half-opening angle α appears as a parameter, and therefore the C_n also depend on α. Numerical values of the C_n have been listed in Table 1 for α values ranging from 5 to 40 deg. (opening angles from 10 to 80 deg.).* These results were obtained from solutions of sets of thirteen, fourteen, fifteen, and sixteen linear algebraic equations on an IBM-704 electronic computer (single precision program). The C_n values listed for each α represent those results which were invariant as the number of linear equations was changed. The rapid decrease of the numerical values of the C_n with increasing n is clearly evident from the table.

The C_n thus are available, the dimensional constants A_n are also known [Equation (10)], and with these the velocity distribution can be calculated from Equation (7). Various results of engineering interest will now be derived from the velocity solution.

FRICTION FACTOR—REYNOLDS NUMBER RELATIONSHIP

Of perhaps greatest engineering interest is the relationship between the rate of flow and the pressure drop, which in dimensionless terms may be represented as a relationship between friction factor and Reynolds number. As a starting point in the derivation of this result it is convenient to calculate the mass rate of flow w which passes through the cross section

$$w = \rho \int_A rudrd\theta = 2\rho \int_0^\alpha d\theta \int_0^{s/\cos\theta} rudr \tag{11}$$

To proceed with the calculation the velocity distribution is introduced from Equation (7), and the dimensional constants A_n are replaced by the C_n from Equation (10). After carrying out the integration one gets

$$\frac{w}{\frac{s^4}{4\nu}\left(-\frac{dp}{dx}\right)} = \frac{\tan\alpha}{3}\left(\frac{1}{\cos 2\alpha}-1\right) + \sum_{n=1} 2C_n\left[\frac{(2n-1)\pi}{2\alpha}+2\right]^{-1} I_n \tag{12}$$

where I_n is an abbreviation for

$$I_n = \int_0^\alpha \frac{\cos[(2n-1)\pi\theta/2\alpha]}{[\cos\theta]^{\frac{(2n-1)\pi}{2\alpha}+2}} d\theta \tag{12a}$$

This latter integral cannot be carried out in closed form, and numerical techniques were therefore utilized. The values of I_n thus obtained have been listed in Table 2.* With this tabulation utilized in conjunction with the C_n values of Table 1 the flow-pressure drop ratio appearing on the left side of Equation (12) has been evaluated. Since the C_n and I_n are both functions

TABLE 2. LISTING OF I_n VALUES

α	I_1	I_2	I_3	I_4
5°	0.05637	−0.02234	0.01549	−0.01273
10°	0.11477	−0.05400	0.04330	−0.04099
15°	0.17589	−0.09824	0.09127	−0.09975
20°	0.24055	−0.15971	0.17249	−0.21831
25°	0.30978	−0.24521	0.30924	−0.45535
35°	0.46767	−0.53469	0.93802	−1.9085
40°	0.56047	−0.77980	1.6369	−3.9718

* That is within any coordinate system one coordinate is not constant along each of the bounding walls.

* The isosceles right triangle (α = 45 deg.) has an exact solution which is given in references 1 and 2.

* Values of I_n for $n > 4$ were not needed in computing flow results to four significant figures.

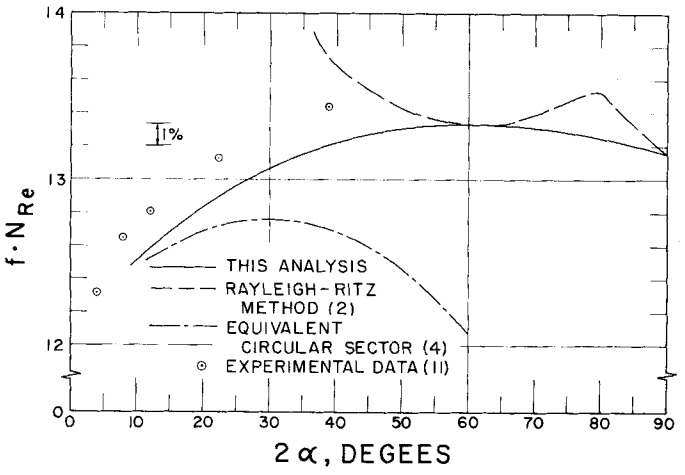

Fig. 2. Friction factor-Reynolds number results.

of the duct opening angle α, so also is the flow-pressure drop ratio, and from the computations it is found that this functional dependence is a strong one. It is therefore desirable to rephrase the flow-pressure drop results into a form which is independent of α, or at least which only depends weakly on α. To this end the friction factor and Reynolds number will be introduced.

If an overall force balance is carried out for the cross section as a whole, it follows that

$$(-dp)A = \bar{\tau} P\, dx \qquad (13a)$$

Next a friction coefficient* f is defined as

$$f = \bar{\tau}/\tfrac{1}{2}\rho\bar{u}^2 \qquad (13b)$$

in which $\bar{u}$ is given by

$$\bar{u} = w/\rho A \qquad (13c)$$

Combining equations (13*a*) and (13*b*) one obtains

$$-dp/dx = \frac{2\rho\bar{u}^2}{D_h} f \qquad (13d)$$

The hydraulic diameter D_h for the triangular duct is

$$D_h = 4A/P = 2s[\sin\alpha/(1 + \sin\alpha)] \qquad (13e)$$

Finally, after eliminating the average velocity $\bar{u}$ from Equation (13*d*) in favor of the mass flow w and noting that the cross-sectional area $A = s^2 \tan\alpha$, one gets

$$f \cdot N_{Re} = \frac{8 \tan\alpha \sin^2\alpha}{(1 + \sin\alpha)^2} \left[\frac{w}{\frac{s^4}{4\nu}\left(-\frac{dp}{dx}\right)} \right]^{-1} \qquad (14)$$

where the N_{Re} is the Reynolds number $\bar{u}D_h/\nu$.

Inspection of this expression reveals that the friction factor-Reynolds number product is related to the reciprocal of the flow-pressure drop ratio of Equation (12). The numerical values calculated from Equation (12) may then be substituted into Equation (14) and the $f \cdot N_{Re}$ product thus determined.

The friction factor-Reynolds number results have been plotted on Figure 2 (solid curve) as a function of duct opening angle ranging from 10 to 90 deg. If one takes note of the extremely expanded ordinate scale, it is seen that the $f \cdot N_{Re}$ product has a remarkably small variation with opening angle, ranging from about 12.5 at $2\alpha = 10$ deg. to a maximum of 13.33. It would thus appear that the hydraulic diameter is quite effective in rationalizing the geometrical differences between isosceles ducts of different opening angles. It should be noted however that the hydraulic diameter does not bring the triangular duct results together with those of circular ducts, the latter being $f \cdot N_{Re} = 16$.

Figure 2 contains all the information needed to calculate the pressure drop in the triangular duct. Entering the figure with opening angle α, one gets the corresponding $f \cdot N_{Re}$ from the curve. Once the Reynolds number has been calculated, the pressure drop is obtained from Equation (13*d*).

Comparison With Other Analyses and Experiment

In addition to the solid curve representing the results of the present analysis Figure 2 also shows the results of prior analytical and experimental studies. The dashed curve was derived by Nuttall (*3*) by means of the approximate Rayleigh-Ritz variational method. Actually Nuttall's work was concerned with the torsion problem for a triangular cross section, and the results were originally reported as twisting moments. The stress function in the torsion problem is governed by the same differential equation as the velocity distribution for fully developed duct flow, and therefore it has been possible to convert the twisting moment results into the friction factor-Reynolds number product. Inspection of the figure reveals that as the apex angle decreases below 60 deg., the friction factor-Reynolds number product from approximate Rayleigh-Ritz solution increases rather rapidly, with growing deviations from the present results. The inadequacy of the Rayleigh-Ritz solution for smaller opening angles was recognized by Nuttall himself. In the range of opening angles between 60 and 90 deg. the dashed curve displays a somewhat unexpected maximum. This is caused by using two different approximating functions in carrying out the Rayleigh-Ritz calculation in this range.

The dot-dashed curve is based on the analysis of Eckert, Irvine, and Yen (*4*) for the circular sector. In a prior report (*7*) these authors had suggested that the sector results might serve as a reasonable approximation for the triangle, under the condition that the sector radius R was chosen to give a cross-sectional area equal to that of the triangle. This suggestion was made with ducts of small opening angle in mind. The equality of cross-sectional areas for sector and triangle is expressed by $R = s(\tan\alpha/\alpha)^{1/2}$ and when the results of reference *4* are modified by this relation, the dot-dashed curve of Figure 2 is obtained. It is seen from the figure that the results taken from the sector solution are in close agreement with those of the present analysis for small opening angles. As the angle increases, the modified sector results fall increasingly lower than those obtained here for the triangle. This trend is physically reasonable, since the base of an isosceles triangle makes an angle less than 90 deg. with the oblique sides, while the base of a circular sector (that is the circular arc) always meets the oblique sides at 90 deg. Therefore, for the triangle, there is greater frictional resistance in the neighborhood of these corners. Moreover as the apex angle increases, the base angles of an isosceles triangle decrease, thus increasing this frictional resistance.

Finally consideration may be given to experimental results. The triangular-duct, laminar-flow measurements of Nikuradse (*6*) have been appraised in reference *8*, and it is concluded that uncertainties exist. Nikuradse's data will therefore not be used here. References *7* through *11* report on various experimental studies by Eckert, Irvine, and co-workers. The last of these, by Carlson and Irvine, contains the most complete set of triangular-duct, laminar friction factor data, and it is these which are plotted on Figure 2. By inspection of the figure it is seen that the experimental data fall about 1.5%

* This is the same definition as for circular tubes, except that the average shear $\bar{\tau}$ must be used here.

above the present analytical results. From a careful error analysis it is concluded (*11*) that the maximum systematic error was 2.5% for the friction factor and 2.12% for the Reynolds number. Thus, within the limits of experiment accuracy, there is excellent agreement between theory and experiment.

VELOCITY DISTRIBUTIONS

Insight into the flow pattern may be obtained from a presentation of velocity distributions. These may be displayed either as velocity contour diagrams or as velocity profile plots. The velocity at any point r, θ in the cross section is calculable from Equation (7) from which the A_n may be eliminated by use of Equation (10); thus

$$u\left|\frac{s^2}{4\mu}\left(-\frac{dp}{dx}\right)=\left(\frac{r}{s}\right)^2\right. \cdot\left(\frac{\cos 2\theta}{\cos 2\alpha}-1\right)+\sum_{n=1} C_n\left(\frac{r}{s}\right)^{\frac{(2n-1)\pi}{2\alpha}}\cos\left[\frac{(2n-1)\pi\theta}{2\alpha}\right] \tag{15}$$

The constants C_n needed to carry out the calculation are listed in Table 1 as a function of the half-opening angle α.

Velocity contour diagrams for three representative duct opening angles have been prepared and are presented in Figure 3. The three opening angles selected are 20, 40, and 80 deg. (α = 10, 20, and 40 deg.), and to these respectively correspond Figures 3(*a*), 3(*b*), and 3(*c*). In each of these figures only half of the duct is shown, the other half is a mirror image. A velocity contour line represents the locus of points having the same velocity. The contour lines shown in the figures represent constant values of $u/\bar{u}$. The maximum value of $u/\bar{u}$ appears as a single point at the center of the contour pattern. Inspection of the contour diagrams for the three opening angles reveals the following flow pattern. For small opening angles the flow is concentrated in the wide portion of the duct (right-hand part of Figure 3*a*). Also the contour lines are generally closer together in the wide part of the duct. This indicates that the velocity varies more rapidly in the wide part of the duct than in the region of the apex. As the duct opening angle increases, the unbalance of flow between the wide part of the duct and the apex region tends to diminish.

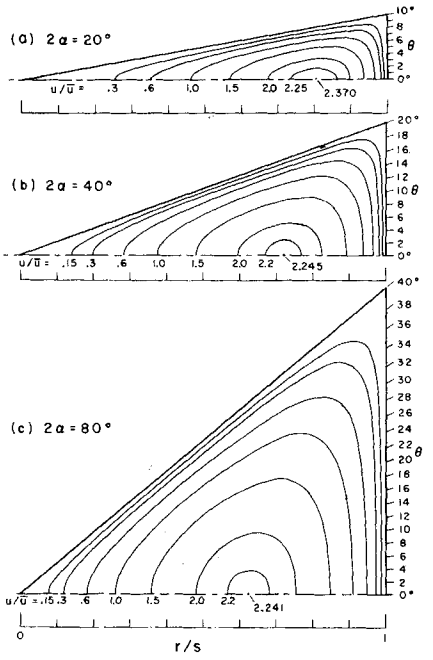

Fig. 3. Representative velocity contour diagram.

This may be verified by noting that the intercept of a given contour line (for example $u/\bar{u} = 1$) with the horizontal symmetry axis moves toward the apex (leftward) as α increases. Another interesting observation which follows from Figure 3 relates to the ratio $u_{max}/\bar{u}$. It would appear that $u_{max}/\bar{u}$ is not a strong function of opening angle, ranging from 2.37 for a 20 deg. opening angle to 2.24 for an 80 deg. opening angle.

An alternate representation of the velocity information may be made by plotting velocity profiles. Owing to space limitations, only a single graph showing typical results has been included. This information is presented on Figure 4, which shows the variation of the velocity along various radial lines (that is lines of constant θ) corresponding to a duct opening angle of 40 deg. (α = 20 deg.). From this figure it is seen that the conclusions already drawn from the velocity contour diagrams are substantiated; the velocities in the neighborhood of the apex (small r/s) are low and the variations of velocity are quite gradual. On the other hand in the wide part of the duct the velocities are high and the variations quite rapid as the duct wall is approached. However certain additional details are available from Figure 4 which perhaps could not so readily be seen in Figure 3. For example, with regard to the largest velocity achieved along the various constant θ lines, Figure 4 indicates that the locations of these maxima shift toward the apex (leftward) as θ decreases, that is as the symmetry line is approached. This is in accordance with physical reasoning.

The velocity contours and profiles of Figures 3 and 4 have been presented to illustrate the nature of the flow pattern. Detailed velocity information for isosceles ducts which have opening angles between 10 and 80 deg. may be obtained by evaluating Equation (15) and making use of the C_n values listed in Table 1. For a duct opening angle of 90 deg. Equation 4-89 of reference *1* may be used.

The velocity solution as found here is given by an expression with a moderate number of terms [Equation (15)] and is, at the same time, highly accurate. It is expected that this solution should prove useful in future velocity-dependent calculations, for example for the heat transfer.

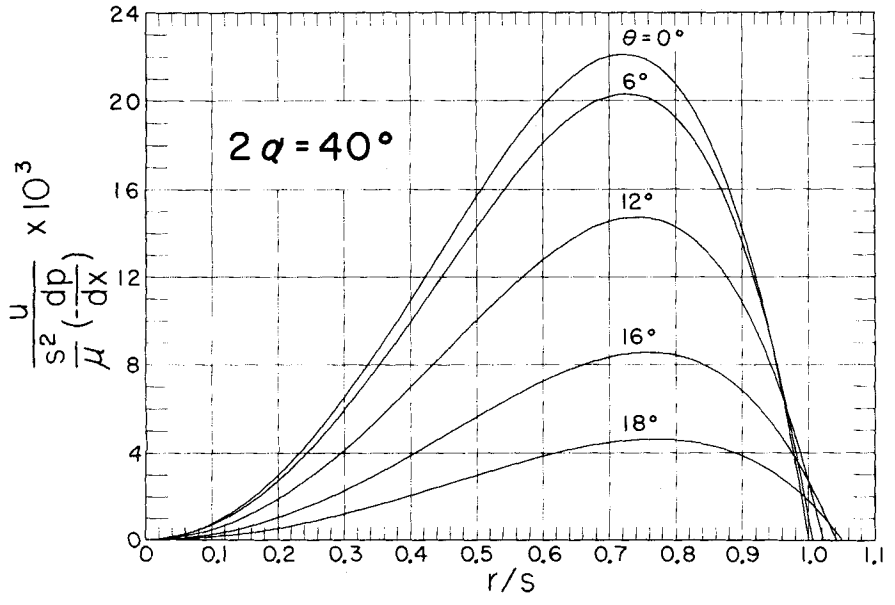

Fig. 4. Velocity profiles for duct with 40 deg. opening angle.

WALL SHEAR STRESS DISTRIBUTIONS

The shear stress exerted by flowing fluid on local positions on the duct wall may be determined by application of the Newtonian shearing law $\tau = \mu(\partial u/$

∂N). On the base surface of the isosceles duct (right-hand boundary, Figure 1) the normal derivative may be expressed in terms of cylindrical coordinates as follows:

$$\frac{\partial u}{\partial N} = \frac{\sin\theta}{r}\frac{\partial u}{\partial \theta} - \cos\theta\frac{\partial u}{\partial r}$$

If one introduces the velocity distribution from Equation (15) and notes that $r = s/\cos\theta$ on the base surface, the shear stress expression is found to be

$$\tau \Big/ \left(-s\frac{dp}{dx}\right) = \frac{1}{2}\left(\frac{1}{\cos 2\alpha} - 1\right) - \frac{1}{4}\sum_{n=1} C_n \frac{(2n-1)\pi}{2\alpha} \cos\left\{\left[\frac{(2n-1)\pi}{2\alpha} - 1\right]\theta\right\} \Big/ \left[\cos\theta\right]^{\frac{(2n-1)\pi}{2\alpha}-1} \qquad (16)$$

With the values of C_n as given in Table 1, Equation (16) has been evaluated to give the shear stress distribution along the base surface. The results thus obtained are plotted on Figure 5 for parametric values of the duct opening angle 2 α. Because symmetry is present about the duct center line, only positive values of the angular position variable θ have been considered; the shear distribution for negative θ values is found by reflecting the graph about the ordinate axis. Inspection of the figure reveals definite trends. First it is seen that for a given pressure drop the wall shear stress at all locations is higher for ducts with larger opening angles. This finding is plausible,* since the velocities at a fixed pressure drop and duct height s are considerably higher in larger opening angle ducts. Additionally for a given duct the highest shear stress on the base surface occurs at the midpoint ($\theta = 0$ deg.). The shear decreases monotonically as the corner region is approached (increasing θ). This too is physically reasonable, since the fluid in the corner region is retarded by two walls (base surface and oblique surface) and therefore has low velocity and correspondingly small velocity gradients. On the other hand fluid adjacent to the midregion of base surface is relatively free to achieve high velocities and correspondingly high gradients.

Next consideration may be given to the shear stress distribution on either of the oblique walls of the isosceles duct, and for concreteness the wall at $\theta = \alpha$ may be taken. On this surface the inward-drawn normal is in the $-\theta$ direction, and so $\tau = -\mu(\partial u/\partial\theta)$. If one introduces the velocity distribution from Equation (15) and sets

$$\tau \Big/ \left(-s\frac{dp}{dx}\right) = \frac{1}{2}\frac{r}{s}\tan 2\alpha + \frac{1}{4}\sum_{n=1} C_n (-1)^{n+1}\frac{(2n-1)\pi}{2\alpha}\left(\frac{r}{s}\right)^{\frac{(2n-1)\pi}{2\alpha}-1} \qquad (17)$$

$\theta = \alpha$ after differentiation, there is obtained

This expression has been numerically evaluated with the C_n from Table 1, and the resulting shear stress distributions are plotted on Figure 6 for parametric values of the duct opening angle 2α. The abscissa represents the distance along the oblique surface as measured from the apex.

From the figure it is seen that, as before, the shear stress (at a given pressure drop) increases with duct opening angle. For any given duct the largest shear on the oblique surface will occur at some location away from the low velocity corner regions ($r = 0$, $r = s/\cos\alpha$). It is interesting to observe that the location of largest shear is quite sensitive to duct opening angle and shifts toward the apex (smaller r/s) as the opening angle increases. This is related to the general increase of the flow in the apex region which accompanies an increase in α.

There is an interesting point of comparison which can be made between Figures 5 and 6 relating to the maximum shear in a duct of given opening angle. For opening angles greater than 60 deg. the maximum shear occurs on the base surface, but for opening angles less than 60 deg. the maximum shear occurs on the oblique surface.

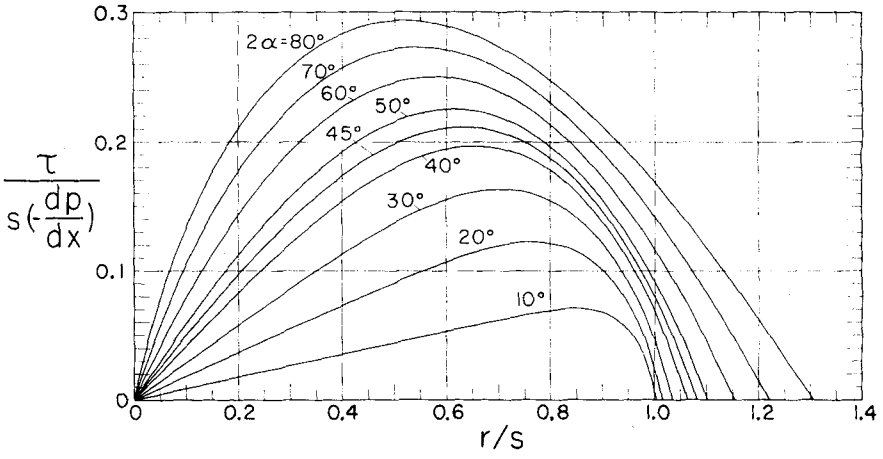

Fig. 6. Shear stress distribution along oblique side of isosceles duct.

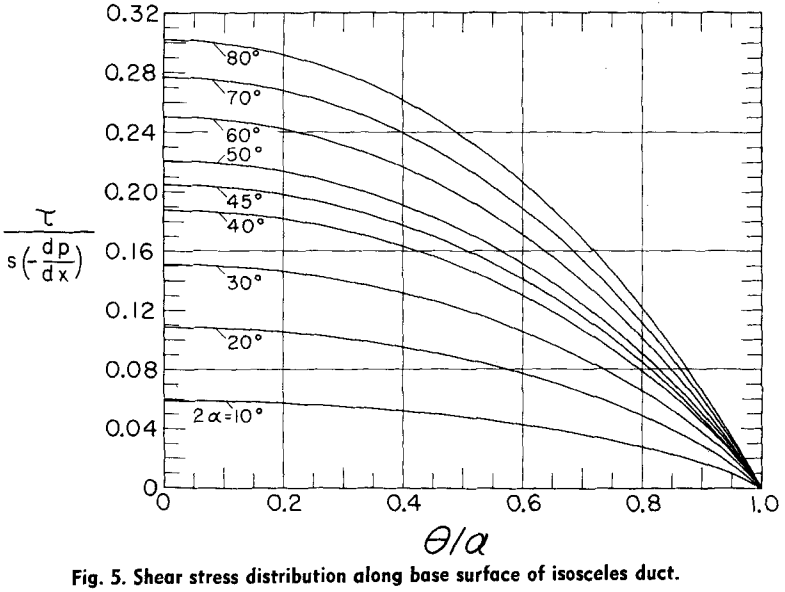

Fig. 5. Shear stress distribution along base surface of isosceles duct.

CONCLUSION

The fully developed laminar flow characteristics for the isosceles triangular duct have been analytically determined to high accuracy. It would be expected that the same analytical method could be employed to determine the fully developed heat transfer characteristics under the condition of axially uniform wall heat flux.

* An alternate, more mathematical explanation may be obtained by substituting Equation (13*e*) into (13*a*); thus

$\bar{\tau} = (-dp/dx)\ (s/2)\ [\sin\alpha/(1+\sin\alpha)]$

For fixed values of dp/dx and s, $\bar{\tau}$ increases with α.

ACKNOWLEDGMENT

This research was supported by a grant from the Graduate School of the University of Minnesota. The author gratefully acknowledges the assistance of the Applied Mathematics Division, Argonne National Laboratory, and particularly of Mr. David L. Russell and Dr. William F. Miller, head of the Division, in connection with the numerical determination of the C_n and I_n. The assistance of Mr. Lawrence S. Jurewicz in other aspects of the numerical work is also gratefully acknowledged.

NOTATION

A_n = dimensional constants
A = cross-sectional area
C_n = dimensionless constants, Table 1
D_h = hydraulic diameter, $4\ A/P$
f = friction factor, $2\bar{\tau}/\rho\bar{u}^2$
I_n = integrals, Equation (12a) and Table 2
k = summation index
n = summation index
N = inward-drawn normal
N_{Re} = Reynolds number, $\bar{u}\ D_h/\nu$
p = static pressure
P = perimeter
R = radius of circular sector
r = radial coordinate
s = height of isosceles duct
u = axial velocity
$\bar{u}$ = average axial velocity
x = axial coordinate
w = mass rate of flow

Greek Letters

α = half opening angle of duct
θ = angular coordinate
μ = absolute viscosity
ν = kinematic viscosity
ρ = density
τ = local wall shear stress
$\bar{\tau}$ = average wall shear stress

LITERATURE CITED

1. Knudsen, J. G., and D. L. Katz, "Fluid Dynamics and Heat Transfer," McGraw-Hill, New York (1958).
2. Claiborne, H. C., *ORNL 1248*, Oak Ridge National Laboratory, Oak Ridge, Tennessee (1952).
3. Nuttall, H. C., *J. Appl. Mechanics*, **19**, 554 (1952).
4. Eckert, E. R. G., T. F. Irvine, Jr., and J. T. Yen, *Trans. Am. Soc. Mech. Engrs.*, **80**, 1433 (1958).
5. Sparrow, E. M., and A. L. Loeffler, Jr., *A.I.Ch.E. Journal*, **5**, 325 (1959).
6. Nikuradse, J., *Ing. Arch.*, **1**, 306 (1930).
7. Eckert, E. R. G., and T. F. Irvine, Jr., *Trans. Am. Soc. Mech. Engrs.*, **78**, 709 (1956).
8. ————, "Proceedings Fifth Midwestern Conference on Fluid Mechanics," p. 122, University of Michigan Press, Ann Arbor, Michigan (1957).
9. ————, *J. Appl. Mechanics*, **25**, 288 (1958).
10. ————, *J. Heat Transfer*, **82**, 125 (1960).
11. Carlson, L. W., and T. F. Irvine, Jr., *ibid.*, **83**, 441 (1961).
12. Deissler, R. G., and M. F. Taylor, *Nat. Advisory Comm. Aeronaut. Tech. Note 4384* (1958).
13. Hildebrand, F. B., "Advanced Calculus for Engineers," Prentice-Hall, Englewood Cliffs, New Jersey (1956).

Manuscript received August 15, 1961; revision received December 15, 1961; paper accepted December 18, 1961.

The Prediction of Vapor-Liquid Equilibrium Constants for Binary Hydrocarbon Systems in the Critical Region

VINOD S. MEHRA and GEORGE THODOS

The Technological Institute, Northwestern University, Evanston, Illinois

A series of reduced state correlations for the prediction of equilibrium constants for the components of binary hydrocarbon systems have been developed utilizing experimental vapor-liquid equilibrium data reported by Kay (7, 8, 9) for the enthane-*n*-heptane, ethane-*n*-butane, and *n*-butane-*n*-heptane systems. Each correlation applies for a specific value of $\tau = T_{bh}/T_{b1}$, the ratio of the normal boiling points of the two components. Plots of β/β° vs. T_R covering the complete range of liquid compositions are presented for values of $\tau = 1.10, 1.20, 1.40, 1.60, 1.80,$ and 2.00. The term β° represents the reduced vapor pressure of the pure substance, while β is the ratio of the pseudo vapor pressure of this substance in the mixture, $K\pi$, to the critical pressure of the mixture.

The correlations presented in this study reproduce the experimental data used in their development with an average deviation of 2.3% for forty-eight points, with the experimental critical constants reported by Kay. The reliability of these correlations has been tested with the propane-isopentane, methane-ethane, and ethane-cyclohexane systems which have τ values in the range included in this study and for which experimental critical constants are available. An average deviation of 5.1% was produced for thirty-six points. In addition the systems methane-propane, propane-benzene, nitrogen-oxygen, and carbon dioxide-*n*-butane were tested with calculated values for their critical constants and produced average deviations of 8.4, 8.2, 9.4, and 20%, respectively.

The concept of the vapor-liquid equilibrium constant as the ratio of vapor and liquid compositions at equilibrium $K = y/x$ was introduced in 1932 by Souders, Selheimer, and Brown (*19*). If both phases behave as ideal solutions, and the vapor is an ideal gas, the equilibrium constant is equal to the ratio of the vapor pressure of the pure component to the total pressure of the system $K = P^\circ/\pi$.

At elevated pressures the vapor is no longer an ideal gas. When one assumes continued ideal solution behavior for both phases, the equilibrium constant can be expressed as the ratio of the fugacities of the pure component in the vapor and liquid phases $K = f_l^\circ/f_v$. In order to obtain the fugacity of the light component in the liquid phase it becomes necessary to extrapolate the vapor pressure of the pure component past its critical temperature. On the other hand the fugacity of the heavy component in the vapor phase can not be obtained ordinarily at pressures greater than its vapor pressure.

Various methods are presented in the literature for the estimation of equilibrium constants, particularly for hydrocarbon systems. Of notable interest are the methods presented by Gamson and Watson (*4*), Smith and Watson (*20*), Organick and Brown (*16*), Prausnitz, Edmister, and Chao (*17*), and the M. W. Kellogg Com-